Research Article GU J Sci, Part A, 10(4): 442-451 (2023) 10.54287/gujsa.1358177

Gazi University
Journal of Science
PART A: ENGINEERING AND INNOVATION
http://dergipark.org.tr/gujsa

Systematic Investigation on the Synergistic Impact of Gallium (Ga)-Boron (B) Co-Doping on the Features of ZnO Films

Kenan OZEL[1*] Abdullah ATILGAN[2]

[1] Department of Electrical and Energy, GAMA Vocational School, Ankara University, Ankara, Türkiye
[2] Department of Energy Systems Engineering, Faculty of Engineering and Natural Sciences, Ankara Yıldırım Beyazıt University, Ankara, Türkiye

Keywords

Co-doped ZnO Thin Film
Ga Doping
B Doping
Spin Coating Method

Abstract

Herein, gallium-boron co-doped ZnO (GBZO) thin films (TFs) of varying percentages of Ga and B doping content were coated on glass slides via spin-coating technique. The impact of doping content on the features of GBZO TFs was comprehensively probed in this work. The characterization results demonstrate that the doping content has a profound impact on the features of GBZO TFs. The X-ray diffraction results verify the polycrystalline nature of GBZO TFs with varying diffraction peak intensities. AFM images disclose the smooth coating of GBZO TFs with low surface roughness. UV–Vis-NIR transmittance spectra reveal that the deposited TFs exhibit high transparency over 86 % in range of 400-800 nm wavelength with excellent optical properties. The electrical resistance measurements indicate that GBZO TFs having doping concentrations of 2.5 at. % of Ga and 0.5 at. % of B has the lower resistivity, and the resistivity of the samples are strongly affected by the doping content. The obtained knowledge from this study could be useful for the fabrication of TF based optoelectronic devices.

Cite

Ozel, K., & Atılgan, A. (2023). Systematic Investigation on the Synergistic Impact of Gallium (Ga)-Boron (B) Co-Doping on the Features of ZnO Films. *GU J Sci, Part A, 10*(4), 442-451. doi:10.54287/gujsa.1358177

Author ID (ORCID Number)

0000-0002-0250-3731 Kenan OZEL
0000-0002-5624-3664 Abdullah ATILGAN

Article Process

Submission Date 13.09.2023
Revision Date 14.11.2023
Accepted Date 04.12.2023
Published Date 12.12.2023

1. INTRODUCTION

Metal oxides are popularly utilized materials for the design of various electronic and optoelectronic devices extending from transparent transistor to photovoltaic cells (Chen & Lan, 2019; Ozel & Yildiz, 2021a, 2022). Of the metal oxides, zinc oxide (ZnO) is at the centre of intense investigations thanks to its desirable features including high transparency, wide band gap, high electron mobility, low-cost production, facile preparation procedures, high stability, nontoxicity etc. (Yildiz et al., 2012). Notwithstanding, the investigations on the undoped ZnO have disclose the fact that tuning the features of undoped ZnO makes it eligible candidate for various applications (Kara et al., 2017). One of the effective strategies is the incorporation of dopant elements, especially trivalent cations such as Al, In, B, and Ga, into the structure of undoped ZnO (Shukla et al., 2006; Zhao et al., 2022). Among the trivalent cations, boron could effectively modify the features of ZnO TFs because of its lowest ionic radius and greatest electronegativity (Tsay & Hsu, 2013). In addition, it has been reported in some studies that boron doping reduces degradation and provides stable electrical properties (Chen et al., 2007; Steinhauser et al., 2008). Moreover, gallium has been frequently preferred elements for doping of ZnO TFs owing to its higher resistance to oxidation and greater electronegativity (Tsay et al., 2012). Therefore, the synergistic effect of these dopant elements may be effective in adjusting the features of ZnO TFs.

In recent years, the increasing need for sensor-based technologies has led to diversity in sensor architectures and increased efforts to develop highly sensitive TF based sensors with a low-cost production. Specifically,

*Corresponding Author, e-mail: kozel@ankara.edu.tr

ZnO is popular conductive oxides employed in sensor fabrication. Soltabayev et al. (2021) reported Ni doped ZnO TFs can be utilized in NO gas sensing applications. Lee at al. (2021) achieved to obtain ZnO TF based piezo pressure sensor. Dash et al. (2018) reported the production and characterization of photonic crystals based on AZO that can be used in sensor production.

To date, the properties of single-doped ZnO TFs have been comprehensively ascertained, whereas the features of co-doped ZnO TFs have been poorly reported (Kara et al., 2016). Hence, it remains a challenge to fully analyze the synergistic impact of co-additive atoms on the features of ZnO TFs. To optimize GBZO TFs for device fabrication, it is of utmost importance to comprehend their morphological, structural, optical, and electrical characteristics. According to our observation, there is no reported work that has focused on the effect of varying gallium and boron content on GBZO TFs.

In the present study, we concentrated our effort on understanding the effectivity of co-additive atoms on the features of ZnO TFs. In this regard, GBZO TFs with varying percentages of Ga and B doping content were spin-coated on glass slides. The features of the GBZO TFs were systematically examined by measurements made with some characterization systems.

2. MATERIAL AND METHOD

The solutions for the deposition of GBZO TFs were prepared with different percentages of Ga and B doping content. The concentration of dopant elements in the solutions ([Ga+B]/([Ga+B]+[Zn])) was fixed to 3 at. %. First, 0.4 M/l of zinc acetate dihydrate, various at. % of gallium nitrate hydrate (i.e., 3, 2.75, 2.5, 2.25 and 2 at. %) and various at. % of trimethyl borate ($C_3H_9BO_3$; Merck) (i.e., 0, 0.25, 0.5, 0.75 and 1 at. %) were dissolved in methanol (CH_3OH; Merck) and monoethanolamine was added into the solutions. To maintain high transparency and homogeneity for the prepared solutions of co-doped ZnO, they were agitated for 2 h at 60°C utilizing a hot&plate. After aging for 48 h, the resulting solutions were coated on glass slides at a velocity of 2000 rpm for 30 s. Ten cycles of spin-coating and pre-heating at 500°C were realized to get the GBZO TFs. Finally, annealing process was fulfilled at 500°C for 1 h to attain polycrystalline TFs. Hereafter, the obtained co-doped ZnO thin films having doping concentrations of 3 at. % of Ga and 0 at. % of B, 2.75 at. % of Ga and 0.25 at. % of B, 2.5 at. % of Ga and 0.5 at. % of B, 2.25 at. % of Ga and 0.75 at. % of B, 2 at. % of Ga and 1 at. % of B content are called GBZO-1, GBZO-2, GBZO-3, GBZO-4, and GBZO-5, respectively. The dopant contents and boron/gallium doping ratios in the deposited film are given in Table 1.

Table 1. *The dopant contents and boron/gallium doping ratios in the co-doped ZnO TFs*

Sample	Ga ratio (at. %)	B ratio (at. %)	B/Ga ratio (%)	Total dopant ration (at. %)
GBZO-1	3	0	0	3
GBZO-2	2.75	0.25	9	3
GBZO-3	2.5	0.5	20	3
GBZO-4	2.25	0.75	33	3
GBZO-5	2	1	50	3

The crystal structures and structural features of GBZO TFs was unveiled by X-rays diffractometry (XRD) measurements. The topographical analyses of GBZO TFs were achieved by employing atomic force microscope (AFM). The optical features of GBZO TFs were recorded by UV/VIS spectrophotometer. The resistivities of the obtained TFs were characterized by a four-point probe.

3. RESULTS AND DISCUSSION

XRD patterns for co-doped ZnO TFs with varying percentages of Ga and B doping content are illustrated in Figure 1. The XRD results manifest that the observed diffraction peaks are matched with the hexagonal structure of ZnO. As seen, the deposited GBZO films exhibit six diffraction peaks, indicating the polycrystal nature of the films (Serin et al., 2017). The intensity of these peaks changes with doping concentrations of Ga and B elements. Note that our findings are compatible with the results of reported works (Yoshino et al., 2005; Serin et al., 2011).

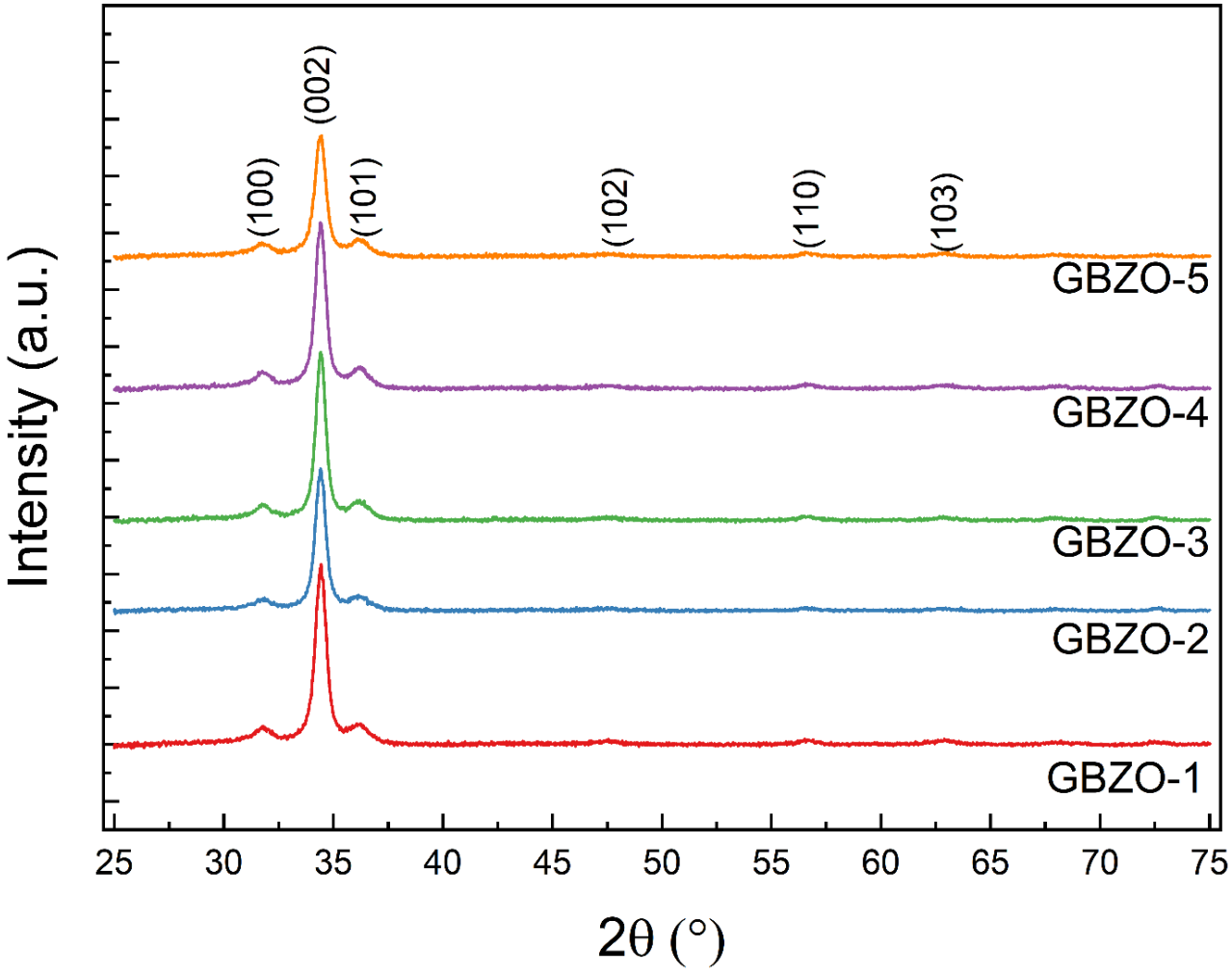

Figure 1. *X-ray diffractogram for GBZO TFs having different percentages of Ga and B content*

An evaluation of the grain size (L) of GBZO TFs by Debye Scherrer equation yields to be in the range of ~14–17 nm. The Debye Scherrer equation is depicted as the following formula (1) (Yildiz et al., 2016).

$$L = \frac{0.9\lambda}{B\cos\theta} \tag{1}$$

Here, λ, B and θ denote the X-rays wavelength (0.154 nm), FWHM, and Bragg angle. Moreover, the values lattice strain (ε) induced from the dopant elements in the GBZO TFs are calculated by using the equations given elsewhere (Liu & Zhu, 2019). All the calculated structural parameters for the deposited GBZO films are delineated in Table 2. As observed, the values of D slightly vary with the doping content and the values of ε increased to some extent with the changes of doping concentrations. As well known, the values of lattice strain strongly affected by the types and concentrations of the doping elements (Zhang et al., 2016).

Table 2. *Obtained parameters for the deposited GBZO films*

Sample	B/dopant ratio	2θ (°)	L (nm)	ε x10-3	Tav (%) (400-800nm)	T (%) @550nm	Eg (eV)
GBZO-1	0	34.42	14.9	0.8986	87.7	93.0	3.278
GBZO-2	0.08	34.41	15.6	1.2853	88.6	94.0	3.280
GBZO-3	0.17	34.42	16.6	1.0905	88.1	86.8	3.283
GBZO-4	0.25	34.40	14.8	1.5057	86.8	87.9	3.275
GBZO-5	0.33	34.41	15.9	1.1440	88.2	91.5	3.273

Figure 2 depicts the 2-dimensional and 3-dimensional AFM images. The surface topographies of the GBZO TFs are characterized with the RMS values which change with the varying doping content. As estimated from AFM images, the RMS values of GBZO TFs are found to be 2.9 nm for GBZO-1, 2.0 nm for GBZO-2, 1.8 nm for GBZO-3, 3.3 nm for GBZO-4 and 3.0 nm for GBZO-5, respectively. Table 3 summarizes the obtained structural and optical parameters for the deposited GBZO TFs. As seen, there is no obvious variation in the surface roughness values of GBZO TFs having different percentages of Ga and B doping content. The lower rougness values indicate that the deposited films possess very smooth surfaces, which ensures high transparency (Farrag & Balboul, 2017). Furthermore, the volume values of the GBZO TFs are calculated to be at around ~13-23 μm^3.

Table 3. *Structural and optical parameters for the deposited GBZO films*

Sample	B/dopant ratio	RMS (nm)	Volume (μm^3)	Thickness (nm)	Resistivity (Ω.cm)	R/T (MΩ)
GBZO-1	0	2.9	18.1	615	150.7	2.45
GBZO-2	0.08	2.0	13.3	615	196.7	3.20
GBZO-3	0.17	1.8	17.0	560	131.5	2.35
GBZO-4	0.25	3.3	22.6	662	170.5	2.58
GBZO-5	0.33	3.0	17.8	596	166.9	2.80

UV–Vis-NIR transmittance *vs.* wavelength profiles of GBZO TFs are delineated in Figure 3. From the profiles, one can observe that the transparency of GBZO TFs is above 86 % in wavelength region of 400-800 nm, which enables the investigated films suitable for optoelectronic applications (Al-Ghamdi et al., 2014). Note that the well-specified interference fringe patterns of the transmittance spectra notify the high-optical-quality of GBZO TFs (Kaur et al., 2015). The calculated average transparency between 400 nm and 800 nm and the transparency at 550 nm of GBZO TFs are given in Table 2. Based on the calculated parameters, one can infer that GBZO-2 exhibits the highest transparency of 94 %, suggesting this film highly suitable for the utilization as a window layer for the fabrication of photovoltaic cells and transparent electronics devices (Kaur et al., 2015).

Thickness of GBZO TFs can be extracted from transmittance profiles by utilizing the following equations (2-4) (Mártil & Díaz, 1992);

$$T_{min} = \frac{6n^2}{(n^4 + 3.25n^2 + 2.25)} \quad (2)$$

$$2nt = (h + 1/2)\lambda_{max} \quad (3)$$

$$2nt = h\lambda_{max} \quad (4)$$

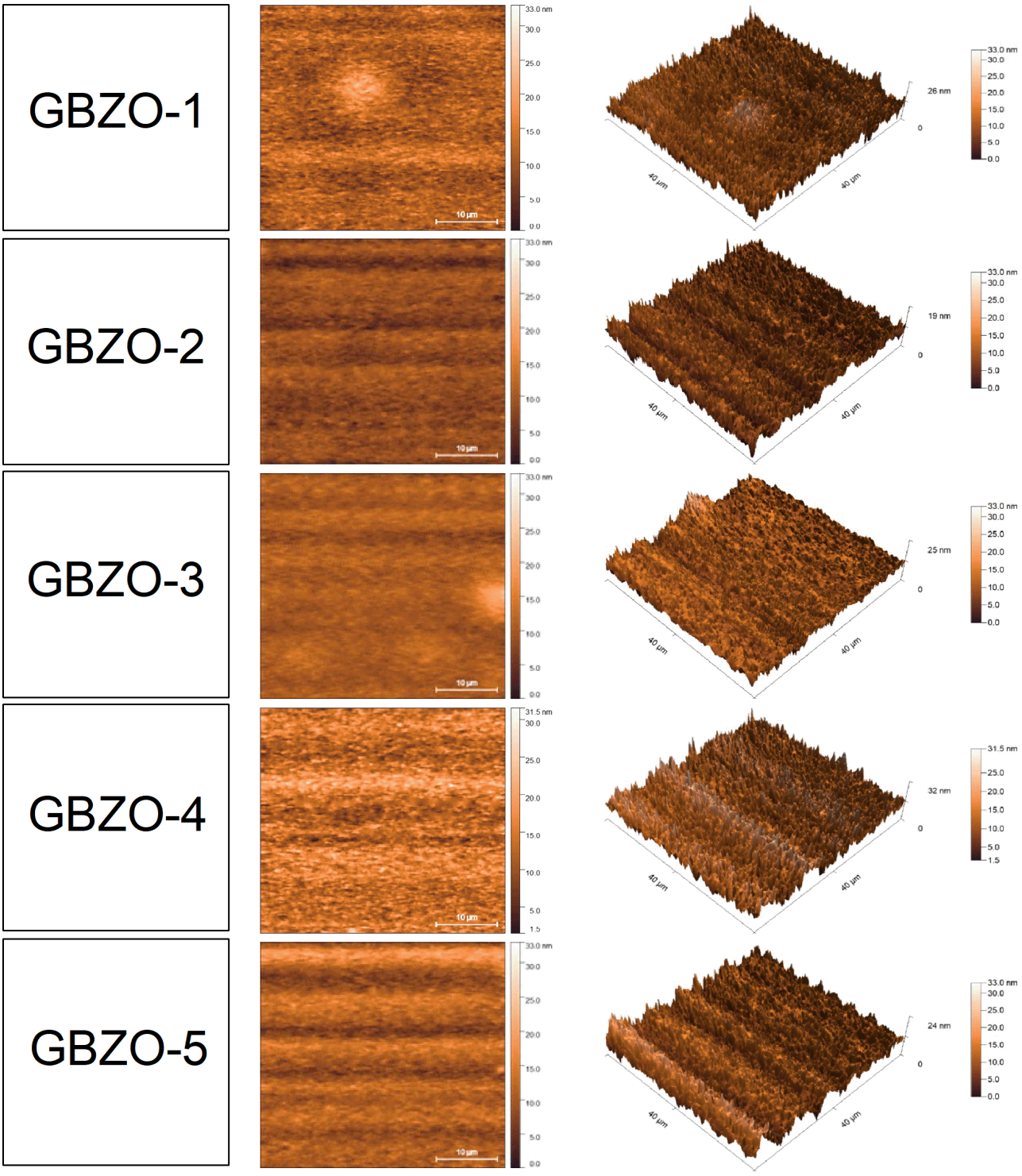

Figure 2. *AFM images of GBZO TFs with different percentages of Ga and B content*

Where T_{min}, n and h stand for the transmittance minima in the optical pattern, refractive index value of the investigated thin film, interface order, respectively. By solving the equation (1), the n values of the films can be obtained. The values of thickness (t) of the GBZO films can be obtained by substituting the n values of TFs in equations (2) and (3). The determined values of t of the investigated TFs are listed in Table 3.

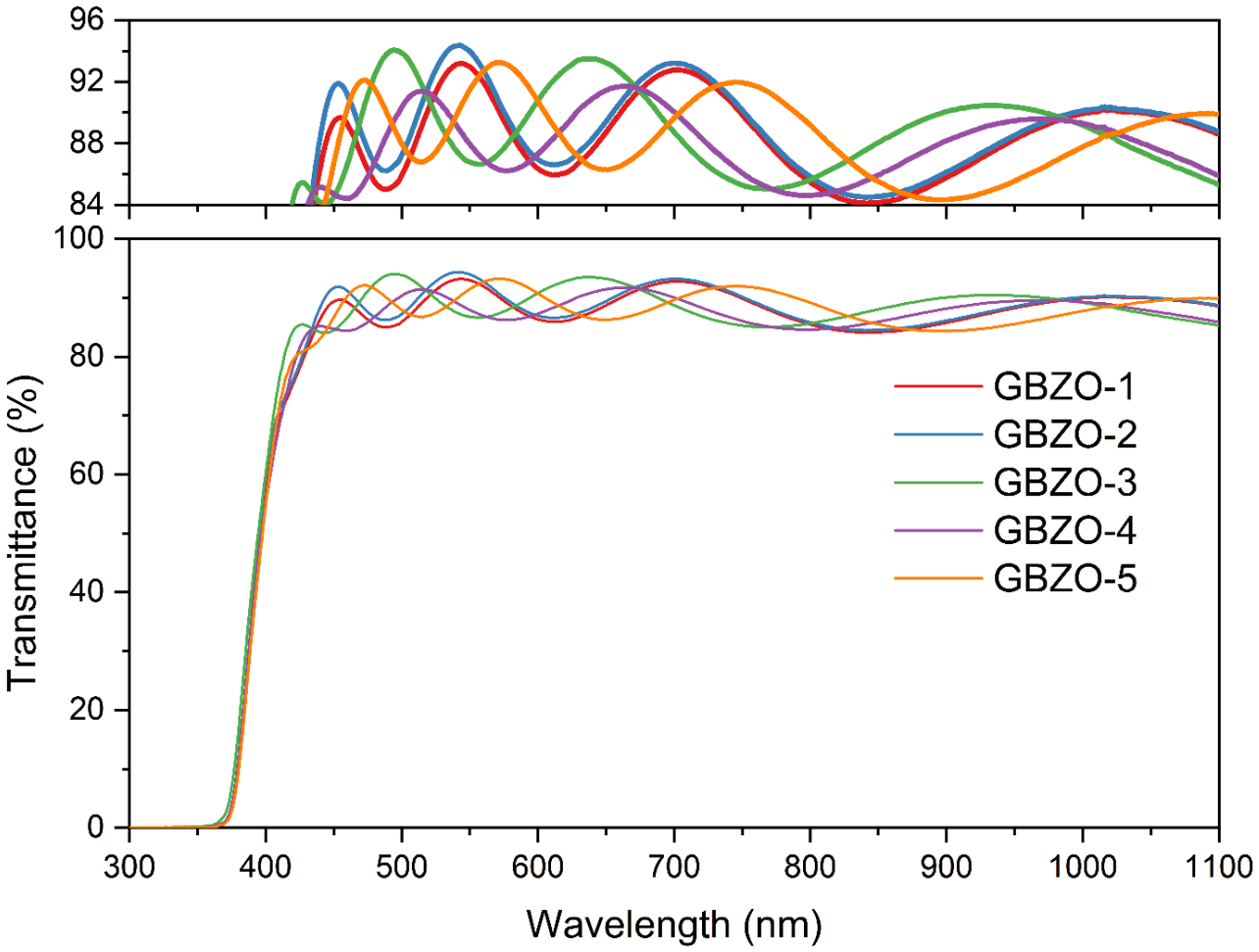

Figure 3. *UV–Vis-NIR transmittance vs. wavelength profiles of GBZO TFs*

Figure 4 illustrates the plots of $(\alpha h\upsilon)^2$as a function of $h\upsilon$ for the investigated GBZO films. Herein, the values of absorption coefficient (α) for GBZO TFs can be extracted from the transmittance data by utilizing Lambert's formula (5) (Choi et al., 2013);

$$\alpha = \frac{1}{t}\ln\left[\frac{1}{T}\right] \tag{5}$$

where T denotes the transmittance of GBZO TFs. The band gap energy (E_g) values of GBZO TFs are calculated by implementing Tauc's equation (6) (Ozel & Yildiz, 2021b);

$$\alpha h\upsilon = D(h\upsilon - E_g)^n \tag{6}$$

where $h\upsilon$ symbolizes the photon energy and D signify the band edge constant. If n=1/2, linear dependence of $(\alpha h\upsilon)^2$ versus $h\upsilon$ is observed in the band edge region, which implies the existence of the direct allowed transition. The extrapolation of linear region in the plots of $(\alpha h\upsilon)^2$ as a function of $h\upsilon$ allows us to extract the values of E_g for GBZO TFs. The extracted values of E_g for the investigated films are found to be as 3.278, 3.280, 3.283, 3.275 and 3.273 eV for GBZO-1, GBZO-2, GBZO-3, GZBO-4 and GBZO-5, respectively and

shown in Table 2. From the results, it can be said that the E_g values of GBZO TFs slightly change with varying content of Ga and B elements.

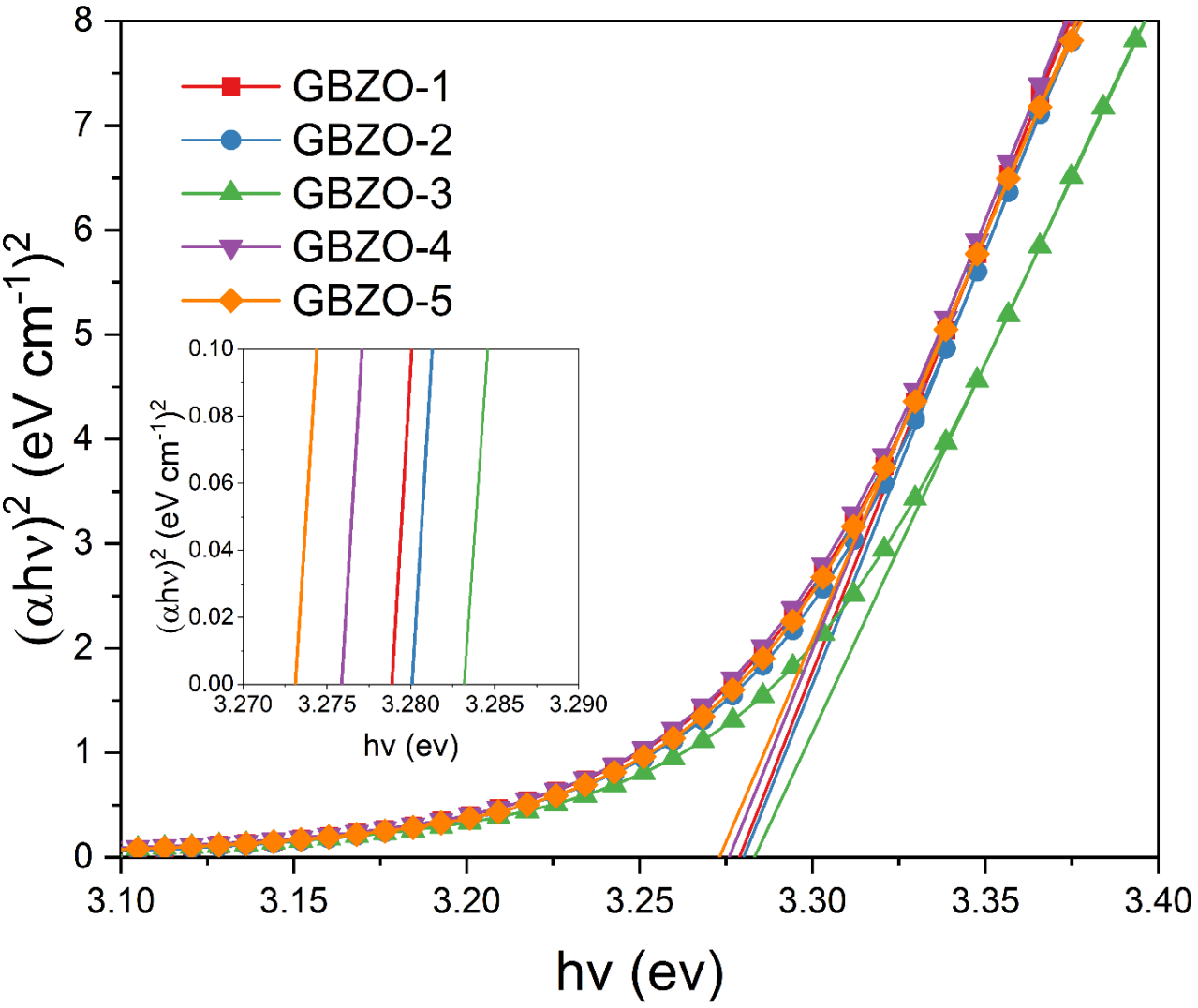

Figure 4. *The plots of* $(\alpha h\upsilon)^2$ *as a function of* $h\upsilon$ *for the investigated GBZO films*

Figure 5 manifests the variation graphs of resistivity (*R*) and sheet resistance (*R/T*) values against Ga doping content in GBZO TFs. The estimated parameters are summarized in Table 3. From the results, one can clearly observe that the GBZO TF with Ga doping content of 2.5 at. % (i.e., GBZO-3; 2.5 at. % of Ga and 0.5 at. % of B) has the lower values of resistivity (*R*) and sheet resistance (*R/T*). Moreover, one can notice that the *R* values decrease with increasing *t* values. The lower value of *R* of GBZO-3 also results from smooth surface and better crystallinity of the sample because the rough surface and low crystallinity deteriorate the flow of electrons (Kaur et al., 2015).

In summary, the features of ZnO TFs can be effectively tuned by co-doping process. Although there are many reported papers on pure and doped ZnO TFs, but a gap exists in literature considering the synergistic impact of gallium and boron co-doping on the features of ZnO TFs. Comparing the experimental findings with the reported studies, one can observe that the characteristic features including grain size, transparency, band gap size, surface roughness, electrical resistivity values of our films are in harmonies with the reported ones (Tsay et al., 2010; Chahmat et al., 2014; Mahroug et al., 2014). Moreover, it can be said that tuning doping content leads to considerable modification in the features of ZnO TFs. Hence, it can be emphasized that the obtained GBZO TFs may be well-qualified for use in different applications such as thin-film-based sensors, photovoltaic cells, and optical filters.

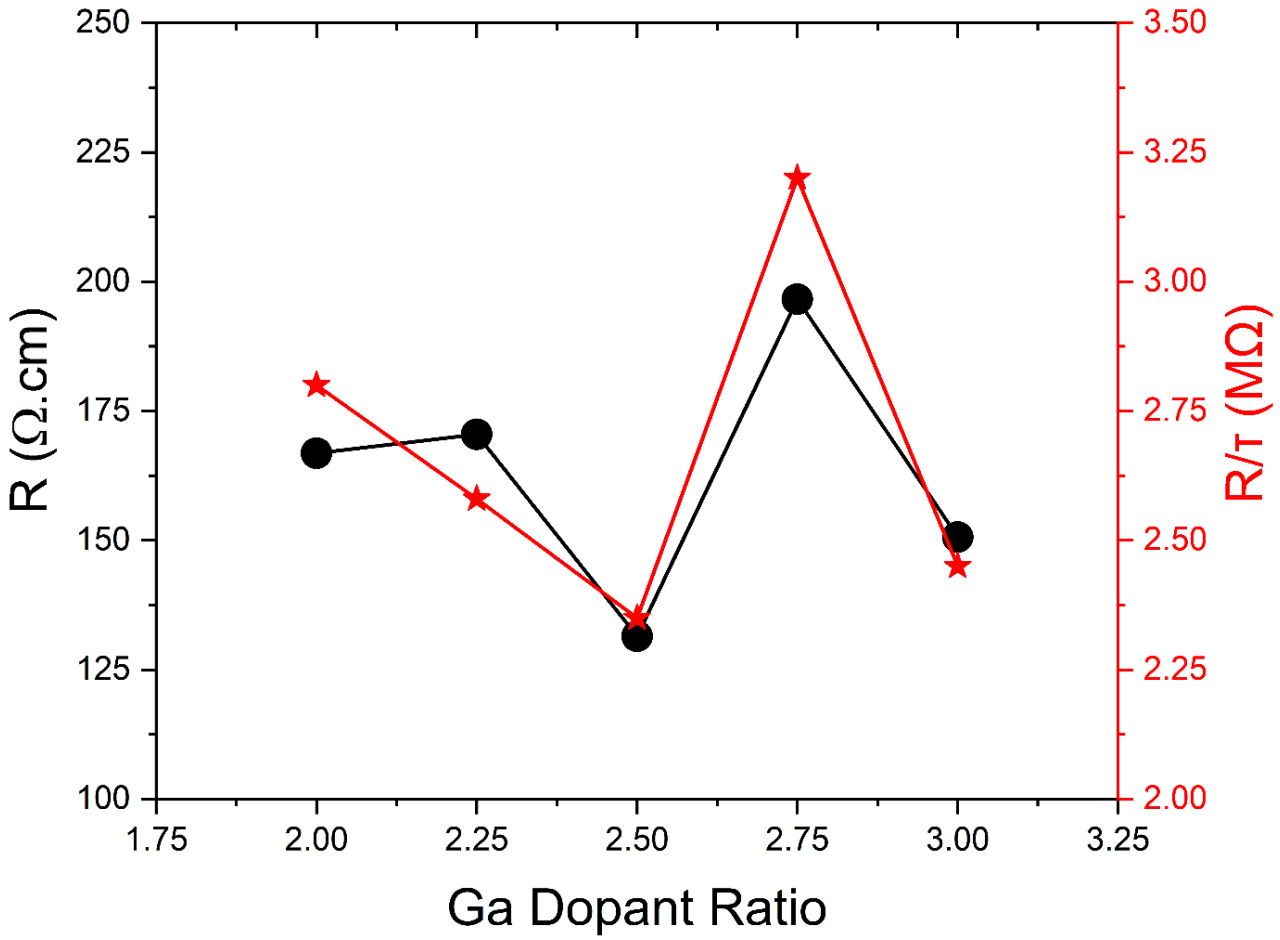

Figure 5. *The graphs of resistivity (R) and sheet resistance (R/T) values against Ga doping content in the GBZO films*

4. CONCLUSION

In summary, the features of GBZO TFs of varying percentages of Ga and B doping content obtained by a spin-coating method were analyzed by various characterization systems. The XRD diffractograms of GBZO TFs demonstrate that the deposited TFs are polycrystalline, demonstrating preferential orientation in (002) plane.

The values of L and ε change with varying doping content because of the difference in the ionic radii of Ga, B and Zn elements. Surface morphology investigations from AFM images show that the deposited films possess very smooth surfaces with small values of RMS. UV–Vis-NIR transmittance profiles of GBZO TFs indicate that the transparency of the deposited TFs is above 86 % in between 400 nm and 800 nm. The t and E_g values of the TFs is extracted from their transmittance data. The electrical resistance measurements point out that the electrical conduction features of the TFs are mightily dependent to their morphological, structural, physical properties. As a result, we can tune the features of co-doped ZnO TFs by changing the doping content and ensure their applicability to different optoelectronic applications.

ACKNOWLEDGEMENT

We would like to thank Professor Abdullah Yildiz and Professor Mohamed Sbeta for providing the necessary laboratory facilities for the realization of this investigation.

CONFLICT OF INTEREST

The authors declare no conflict of interest.

REFERENCES

Al-Ghamdi, A. A., Al-Hartomy, O. A., El Okr, M., Nawar, A. M., El-Gazzar, S., El-Tantawy, F., & Yakuphanoglu, F. (2014). Semiconducting properties of Al doped ZnO thin films. *Spectrochimica Acta Part A: Molecular and Biomolecular Spectroscopy*, *131*, 512-517. https://www.doi.org/10.1016/j.saa.2014.04.020

Chahmat, N., Souier, T., Mokri, A., Bououdina, M., Aida, M. S., & Ghers, M. (2014). Structure, microstructure and optical properties of Sn-doped ZnO thin films. Journal of alloys and compounds, *593*, 148-153. https://www.doi.org/10.1016/j.jallcom.2014.01.024

Chen, X. L., Xu, B. H., Xue, J. M., Zhao, Y., Wei, C. C., Sun, J., Wang, Y., Zhang, X. D., & Geng, X. H. (2007). Boron-doped zinc oxide thin films for large-area solar cells grown by metal organic chemical vapor deposition. Thin Solid Films, *515*(7-8), 3753-3759. https://www.doi.org/10.1016/j.tsf.2006.09.039

Chen, R., & Lan, L. (2019). Solution-processed metal-oxide thin-film transistors: A review of recent developments. *Nanotechnology*, *30*(31), 312001. https://www.doi.org/10.1088/1361-6528/ab1860

Choi, Y. J., Gong, S. C., Johnson, D. C., Golledge, S., Yeom, G. Y., & Park, H. H. (2013). Characteristics of the electromagnetic interference shielding effectiveness of Al-doped ZnO thin films deposited by atomic layer deposition. *Applied Surface Science*, *269*, 92-97. https://www.doi.org/10.1016/j.apsusc.2012.09.159

Dash, J. N., Das, R., & Jha, R. (2018). AZO coated microchannel incorporated PCF-based SPR sensor: a numerical analysis. IEEE Photonics Technology Letters, *30*(11), 1032-1035. https://www.doi.org/10.1109/LPT.2018.2829920

Farrag, A. A. G., & Balboul, M. R. (2017). Nano ZnO thin films synthesis by sol–gel spin coating method as a transparent layer for solar cell applications. *Journal of Sol-Gel Science and Technology*, *82*, 269-279. https://www.doi.org/10.1007/s10971-016-4277-8

Kara, I., Atilgan, A., Serin, T., & Yildiz, A. (2017). Effects of Co and Cu dopants on the structural, optical, and electrical properties of ZnO nanocrystals. *Journal of Materials Science: Materials in Electronics*, *28*, 6088-6092. https://www.doi.org/10.1007/s10854-016-6285-4

Kara, I., Yildiz, A., Yildiz, G., Dogan, B., Serin, N., & Serin, T. (2016). Al and X (Sn, Cu, In) co-doped ZnO nanocrystals. *Journal of Materials Science: Materials in Electronics*, *27*, 6179-6182. https://www.doi.org/10.1007/s10854-016-4546-x

Kaur, G., Mitra, A., & Yadav, K. L. (2015). Pulsed laser deposited Al-doped ZnO thin films for optical applications. *Progress in Natural Science: Materials International*, *25*(1), 12-21. https://www.doi.org/10.1016/j.pnsc.2015.01.012

Lee, P. C., Hsiao, Y. L., Dutta, J., Wang, R. C., Tseng, S. W., & Liu, C. P. (2021). Development of porous ZnO thin films for enhancing piezoelectric nanogenerators and force sensors. *Nano Energy*, *82*, 105702. https://www.doi.org/10.1016/j.nanoen.2020.105702

Liu, Y., & Zhu, S. (2019). Preparation and characterization of Mg, Al and Ga co-doped ZnO transparent conductive films deposited by magnetron sputtering. *Results in Physics*, *14*, 102514. https://www.doi.org/10.1016/j.rinp.2019.102514

Mahroug, A., Boudjadar, S., Hamrit, S., & Guerbous, L. (2014). Structural, optical and photocurrent properties of undoped and Al-doped ZnO thin films deposited by sol–gel spin coating technique. Materials Letters, *134*, 248-251. https://www.doi.org/10.1016/j.matlet.2014.07.099

Mártil, I., & Díaz, G. G. (1992). Undergraduate laboratory experiment: Measurement of the complex refractive index and the band gap of a thin film semiconductor. *American Journal of Physics*, *60*(1), 83-86. https://www.doi.org/10.1119/1.17049

Ozel, K., & Yildiz, A. (2021a). Comprehensive understanding of the role of emitter layer thickness for metal–oxide–semiconductors based solar cells. *IEEE Journal of Photovoltaics*, *12*(1), 251-258. https://www.doi.org/10.1109/jphotov.2021.3119612

Ozel, K., & Yildiz, A. (2021b). The potential barrier-dependent carrier transport mechanism in n-SnO2/p-Si heterojunctions. *Sensors and Actuators A: Physical*, *332*, 113141. https://www.doi.org/10.1016/j.sna.2021.113141

Ozel, K., & Yildiz, A. (2022). Estimation of maximum photoresponsivity of n-SnO_2/p-Si heterojunction-based UV photodetectors. *Physica Status Solidi (RRL) – Rapid Research Letters*, *16*(2), 2100490. https://www.doi.org/10.1002/pssr.202100490

Serin, T., Atilgan, A., Kara, I., & Yildiz, A. (2017). Electron transport in Al-Cu co-doped ZnO thin films. *Journal of Applied Physics*, *121*(9), 095303. https://www.doi.org/10.1063/1.4977470

Serin, T., Yildiz, A., Uzun, Ş., Çam, E., & Serin, N. (2011). Electrical conduction properties of In-doped ZnO thin films. *Physica Scripta*, *84*(6), 065703. https://www.doi.org/10.1088/0031-8949/84/06/065703

Shukla, R. K., Srivastava, A., Srivastava, A., & Dubey, K. C. (2006). Growth of transparent conducting nanocrystalline Al doped ZnO thin films by pulsed laser deposition. *Journal of crystal growth*, *294*(2), 427-431. https://www.doi.org/10.1016/j.jcrysgro.2006.06.035

Soltabayev, B., Er, İ. K., Yildirim, M. A., Ates, A., & Acar, S. (2021). The Dependence of The Nickel Concentration of ZnO Thin Films for Gas Sensors Applications. *Gazi University Journal of Science Part A: Engineering and Innovation*, *8*(1), 157-165.

Steinhauser, J., Faÿ, S., Oliveira, N., Vallat-Sauvain, E., Zimin, D., Kroll, U., & Ballif, C. (2008). Electrical transport in boron-doped polycrystalline zinc oxide thin films. *physica status solidi (a)*, *205*(8), 1983-1987. https://www.doi.org/10.1002/pssa.200778878

Tsay, C. Y., Fan, K. S., & Lei, C. M. (2012). Synthesis and characterization of sol–gel derived gallium-doped zinc oxide thin films. *Journal of Alloys and Compounds*, *512*(1), 216-222. https://www.doi.org/10.1016/j.jallcom.2011.09.066

Tsay, C. Y., & Hsu, W. T. (2013). Sol–gel derived undoped and boron-doped ZnO semiconductor thin films: preparation and characterization. *Ceramics International*, *39*(7), 7425-7432. https://www.doi.org/10.1016/j.ceramint.2013.02.086

Tsay, C. Y., Wu, C. W., Lei, C. M., Chen, F. S., & Lin, C. K. (2010). Microstructural and optical properties of Ga-doped ZnO semiconductor thin films prepared by sol–gel process. *Thin Solid Films*, *519*(5), 1516-1520. https://www.doi.org/10.1016/j.tsf.2010.08.170

Yildiz, A., Serin, T., Öztürk, E., & Serin, N. (2012). Barrier-controlled electron transport in Sn-doped ZnO polycrystalline thin films. *Thin Solid Films*, *522*, 90-94. https://www.doi.org/10.1016/j.tsf.2012.09.006

Yildiz, A., Uzun, S., Serin, N., & Serin, T. (2016). Influence of grain boundaries on the figure of merit of undoped and Al, In, Sn doped ZnO thin films for photovoltaic applications. *Scripta Materialia*, *113*, 23-26. https://www.doi.org/10.1016/j.scriptamat.2015.10.004

Yoshino, K., Fukushima, T., & Yoneta, M. (2005). Structural, optical and electrical characterization on ZnO film grown by a spray pyrolysis method. *Journal of Materials Science: Materials in Electronics*, *16*, 403-408. https://www.doi.org/10.1007/s10854-005-2305-5

Zhang, Y., Liu, C., Liu, J., Xiong, J., Liu, J., Zhang, K., Liu, Y., Peng, M., Yu, A., Zhang, A., Zhang, Y., Wang, Z., Zhai, J., & Wang, Z. L. (2016). Lattice strain induced remarkable enhancement in piezoelectric performance of ZnO-based flexible nanogenerators. *ACS Applied Materials & Interfaces*, *8*(2), 1381-1387. https://www.doi.org/10.1021/acsami.5b10345

Zhao, D., Sathasivam, S., Wang, M., & Carmalt, C. J. (2022). Transparent and conducting boron doped ZnO thin films grown by aerosol assisted chemical vapor deposition. *RSC Advances*, *12*(51), 33049-33055. https://www.doi.org/10.1039/D2RA05895B